Laser Frequency and Intensity Stabilization for Advanced LIGO

Evan Hall[1,*]

(LIGO Scientific Collaboration)

[1]*Department of Physics, California Institute of Technology*

Advanced LIGO searches for gravitational wave events using two 4-km Fabry–Pérot Michelson interferometers separated by a 3000 km baseline. Each interferometer is illuminated with up to 125 W of 1064 nm light from a frequency- and intensity-stabilized Nd:YAG laser. This laser is frequency-locked to the interferometer's common-mode arm length, which acts as a 4-km-long reference cavity with a 1 Hz linewidth. This cavity stores hundreds of kilowatts of quiet light, enabling a differential strain measurement that is better than $10^{-23}/\mathrm{Hz}^{1/2}$ at 100 Hz. The interferometers' sensitivity to differential strain is designed to be limited by shot noise, radiation pressure noise, and mirror thermal noise across the astrophysical detection band (10 Hz to 7 kHz).

I. INTRODUCTION

General relativity predicts that any mass distribution with a time-varying quadrupole moment should generate ripples in the curvature of spacetime. These ripples, referred to as gravitational waves (GWs), propagate outward from the mass distribution at the speed of light and carry away energy from the system. GWs are expected to be produced by a variety of astrophysical systems, such as coalescing binary neutron stars or black holes, rotating neutron stars, and supernovae [1]. A GW induces a tidal force in any matter that it passes through: for two free masses separated by a distance L, the relative distance change ΔL induced by the GW is proportional to L. Therefore, a GW is characterized by the strain $h = (\Delta L)/L$ it produces. Additionally, GWs are tensor waves, meaning that they produce a positive strain $+h$ in one spatial direction while simultaneously producing a negative strain $-h$ in an orthogonal direction. Thus, a suitably oriented GW can be detected with a Michelson interferometer.

The Laser Interferometer Gravitational-Wave Observatory (LIGO) consists of two Michelson interferometers—one in Hanford, WA, and another in Livingston, LA—each with arm length $L = 4$ km. Installation and commissioning of the advanced versions of these interferometers started in 2010, and the first astrophysical observing run was conducted from September 2015 to January 2016. During this run, the instruments detected two GW events, each consistent with the coalescence of a binary black hole system [2, 3].

II. OPTICAL TOPOLOGY

The optical topology of the Advanced LIGO interferometers enables a differential strain measurement with an amplitude spectral density (ASD) that is a few parts in $10^{-24}/\mathrm{Hz}^{1/2}$ at 100 Hz [4], limited in large part by the shot noise and radiation pressure noise [5] of the laser light in each interferometer. The optical topology is shown on the right-hand side of fig. 1.

The beamsplitter and end test masses by themselves would form a simple Michelson interferometer with arm length $L = 4$ km. However, if this simple Michelson were illuminated with $P_0 = 125$ W of light with wavelength $\lambda_0 = 1\,\mu$m, the shot-noise-limited strain ASD would be $(hc\lambda_0/2P_0)^{1/2}/2\pi L = 1 \times 10^{-21}/\mathrm{Hz}^{1/2}$, three orders of magnitude worse than the target sensitivity [6].

To improve the Michelson sensitivity, a test mass with transmissivity $T_\mathrm{i} = 1.4\,\%$ is placed in each arm, transforming the arm into a Fabry–Pérot cavity with a finesse $\mathcal{F} = 2\pi/T_\mathrm{i}$ and cavity pole $f_\mathrm{a} = c/4L\mathcal{F}$. This enhances the shot-noise-limited strain sensitivity by $(2\mathcal{F}/\pi)/\sqrt{1 + (f/f_\mathrm{a})^2}$.

The sensitivity can be further enhanced by placing a power-recycling mirror between the laser source and the beamsplitter; this increases the power circulating in the interferometer. The greatest enhancement is achieved by choosing the transmissivity to be $T_\mathrm{p} = 4\eta_\mathrm{a}/T_\mathrm{i}$, where η_a is the round-trip power loss of each arm. This has the additional benefit of narrowing the arm linewidth for common-mode signals only (e.g, laser frequency or intensity noise), so that these signals are filtered as they circulate in the interferometer.

Finally, placing a signal-recycling mirror between the beamsplitter and the GW readout changes the arm linewidth for differential signals only (e.g., from gravitational waves). The mirror may be controlled so as to either broaden or narrow this differential linewidth, allowing the shot noise and the radiation pressure noise to be optimized based on expected astrophysical waveforms [6].

For Advanced LIGO, the arm finesse is chosen to be $\mathcal{F} = 450$ (i.e., $T_\mathrm{i} = 1.4\,\%$), based on expected optical losses and displacement noise couplings from other degrees of freedom [4]. With $\eta_\mathrm{a} = 100$ ppm, this sets $T_\mathrm{p} = 3.0\,\%$, producing a common-mode cavity with finesse 3×10^4 and cavity pole $f_+ = 0.6$ Hz. The signal recycling mirror transmissivity is chosen to be $T_\mathrm{s} = 20\,\%$, and controlled so as to broaden the differential cavity pole to $f_- = 750$ Hz. For 125 W of input power, this yields a shot noise limit of $2.9 \times 10^{-24}/\mathrm{Hz}^{1/2}$ and a radiation pressure noise limit of $(6 \times 10^{-25}/\mathrm{Hz}^{1/2}) \times (100\,\mathrm{Hz}/f)^2$ for $f < f_-$ (fig. 2).

In addition to the main interferometer, several other optical cavities are employed (fig. 1). On the input side of the interferometer, two ring cavities—the pre-modecleaner and the input modecleaner—filter the laser beam's frequency noise, intensity noise, pointing noise, and shape. A two-mirror fused silica reference cavity is also used to frequency stabilize the laser. At the interferometer output, the output modecleaner filters higher-order spatial modes and rf control sidebands before the laser light is sent to the GW readout photodiodes.

* ehall@caltech.edu

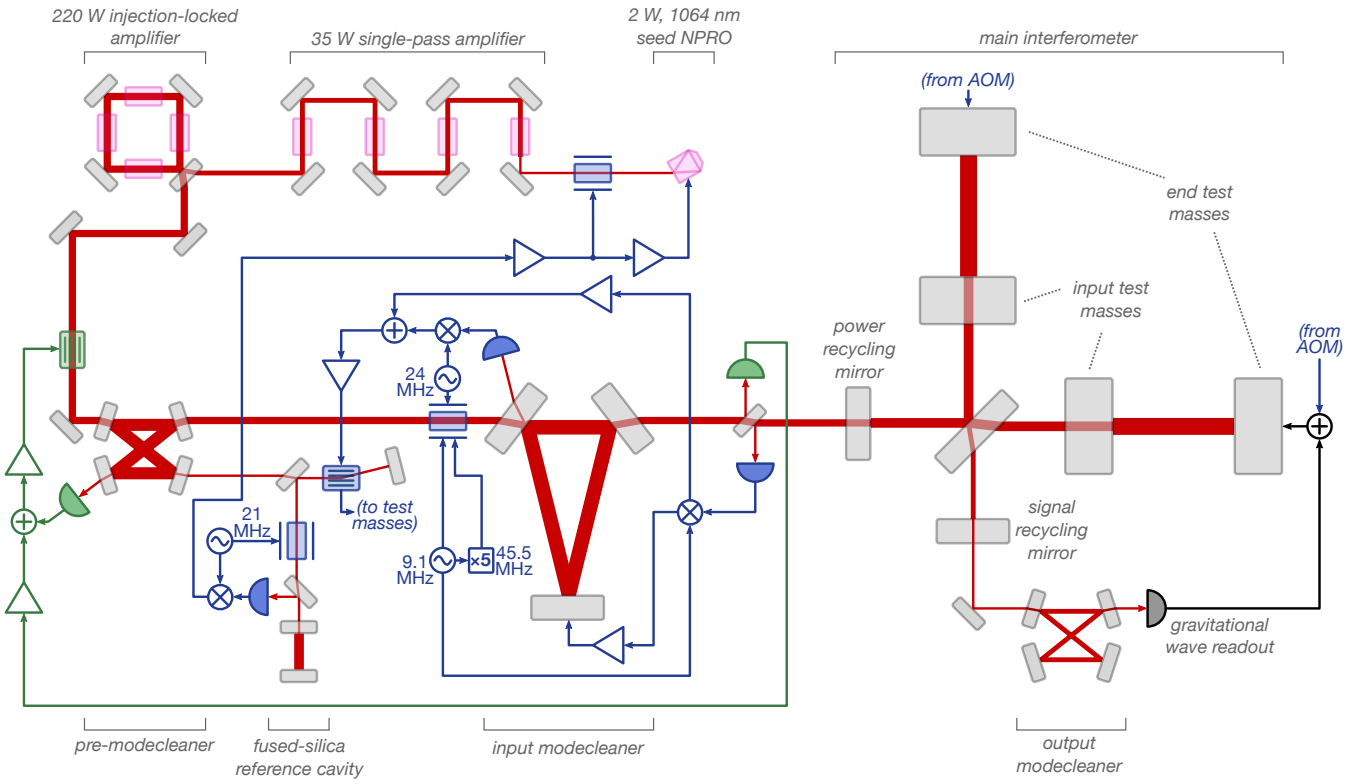

FIG. 1: Diagram of Advanced LIGO, showing the main interferometer, auxiliary optical cavities, and the high-power laser generation. Blue traces show frequency stabilization; green traces show intensity stabilization. Black traces shows the differential arm length control and strain readout. Components for sensing and control of the beamsplitter, recycling mirrors, pre-modecleaner, injection-locked amplifier, and output modecleaner have been omitted. *Key:* photodiode; mixer; electro-optic modulator; acousto-optic modulator; rf oscillator.

III. TEST MASSES, SUSPENSIONS, AND ISOLATION

Each Advanced LIGO test mass is a 40 kg cylinder of polished, low-absorption fused silica. A heavy test mass is desirable to minimize the radiation pressure noise in the interferometer. Silica (SiO_2) and titania-doped tantala (Ta_2O_5) are deposited onto the surface of the test mass via ion-beam sputtering to transform the test mass into a Bragg mirror.

The test mass transmissivity is 4 ppm for the end masses and 1.4 % for the input masses. For both types of test mass, the typical absorption is a few hundred parts per billion. The typical round-trip loss of the arm cavities is approximately 100 ppm in situ [7], suggesting a scatter of 50 ppm per test mass.

In the GW band, the dominant displacement noise arising from the test mass itself is the Brownian thermal noise of the coating [8]; this arises mostly from the modest tantala Q factor—about 4×10^3 [9]. The expected coating noise contribution to the differential strain ASD is about $(2.5\times10^{-24}\,/\mathrm{Hz}^{1/2})\times(100\,\mathrm{Hz}/f)^{1/2}$ [4].

Each test mass is mounted to the bottom of a quadruple pendulum, which provides an isolation transfer function of $(10^{-15}\,\mathrm{m/m})\times(100\,\mathrm{Hz}/f)^8$ in the GW band. To give good thermal noise performance, the penultimate mass is fabricated from fused silica, as are the fibers used to suspend the test mass from the penultimate mass [10]. Brownian noise is expected to dominate the suspension thermal noise in the GW band, with a differential strain ASD of approximately $(5\times10^{-25}/\mathrm{Hz}^{1/2})\times(50\,\mathrm{Hz}/f)^{5/2}$ [4, 10], corresponding to $Q\sim10^9$ for the pendulum longitudinal mode, which has a resonant frequency $f_0 = 0.43$ Hz.

IV. LASER

A. Generation of 220 W beam

The laser is seeded by a commercial Nd:YAG NPRO that produces 2 W of 1064 nm light. Light from this laser enters a single-pass amplifier consisting of four Nd:YVO_4 crystals, yielding 35 W of light. This light is then used to seed an injection-locked ring cavity, which contains four Nd:YAG crystals and yields 220 W of light [11, 12] (fig. 1). All crystals are pumped with 808 nm light; each ring cavity crystal receives 315 W of pump light delivered via 7 fiber-coupled diode lasers. The length of the ring cavity is locked to the seed laser frequency using the Pound–Drever–Hall (PDH) technique [13]. Higher-order mode content from the ring cavity is filtered away by the pre-modecleaner, which is also PDH-locked to the laser frequency. About 125 W of TEM_{00} light is expected to be available to illuminate the interferometer.

B. Frequency stabilization

The desired strain sensitivity of a few parts in $10^{-24}/\mathrm{Hz}^{1/2}$ sets a challenging requirement on the frequency noise of the light used to illuminate the interferometer: the common-mode frequency rejection afforded by the interferometer's Michelson topology is finite due to length, reflectivity, and loss imbalances between the two arms. To ensure that the frequency noise coupling into the GW readout is negligible, the frequency noise at the input to the interferometer must be stabilized to $1\,\mu\mathrm{Hz}/\mathrm{Hz}^{1/2}$ at 100 Hz [14], seven orders of magnitude below the phase noise of a typical freerunning NPRO—about $(100\,\mathrm{Hz}/\mathrm{Hz}^{1/2})\times(100\,\mathrm{Hz}/f)$. In order to achieve this frequency noise requirement, Advanced LIGO employs a multilayered frequency suppression system which exploits the frequency stability of three different optical cavities (fig. 1).

The laser is first stabilized to a 20.3-cm-long tabletop fused silica reference cavity with a 200 kHz servo loop. The PDH error signal is generated by applying 21 MHz phase sidebands and sensing the resulting beat note in reflection of the cavity. This error signal is fed back to the NPRO length (using both strain and thermal actuation), and to a broadband electro-optic modulator placed after the NPRO. Under optimal conditions, the laser's freerunning frequency noise is suppressed down to the Brownian noise level of the reference cavity coatings, about $(6\,\mathrm{mHz}/\mathrm{Hz}^{1/2}) \times (100\,\mathrm{Hz}/f)^{1/2}$ [15].

Next, the laser is stabilized to the suspended input modecleaner with a 50 kHz loop. The error signal is again generated using PDH reflection locking, here using 24 MHz sidebands. Since the modecleaner is a better length reference than the fused silica reference cavity in the GW band, the modecleaner error signal is added to the error point of the tabletop cavity in order to stabilize the laser frequency to the modecleaner. This is accomplished by actuating on a double-pass acousto-optic modulator (AOM) placed at the input to the fused silica cavity. The shot noise of the light on the photodiode limits the frequency noise performance of this loop to a few parts in $10^{-5}\,\mathrm{Hz}/\mathrm{Hz}^{1/2}$.

Finally, the laser frequency is stabilized to the interferometer's common-mode arm length. A PDH error signal is generated in reflection of the interferometer using 9.1 MHz sidebands which resonate between the power recycling mirror and the input test masses. This common-mode error signal is fed back to the modecleaner length. Additionally, the error signal is summed directly into the electronic error point of the modecleaner loop, allowing the laser frequency to be stabilized to the interferometer common-mode length with a bandwidth of 15 kHz. The noise performance of this loop is limited by the shot noise on the PDH photodiode; with a power of 25 W into the interferometer, this amounts to a frequency noise of approximately $1\,\mu\mathrm{Hz}/\mathrm{Hz}^{1/2}$ from 10 to 100 Hz, rising like f above 100 Hz. This input frequency noise is passively filtered above the common-mode cavity pole $f_+ \simeq 0.6$ Hz. This attenuates the frequency noise at 100 Hz to less than $10^{-8}\,\mathrm{Hz}/\mathrm{Hz}^{1/2}$ for the light circulating inside the interferometer.

C. Intensity stabilization

The relative intensity noise (RIN) of the light exiting the injection-locked high power oscillator is typically $10^{-5}/\mathrm{Hz}^{1/2}\times(100\,\mathrm{Hz}/f)$ or better below 1 kHz. On the other hand, an input RIN of less than $1\times10^{-7}/\mathrm{Hz}^{1/2}$ at 100 Hz and $2\times10^{-9}/\mathrm{Hz}^{1/2}$ at 10 Hz is needed in order to make laser intensity fluctuations contribute negligibly to the GW signal [14]. Two dc-coupled servo loops are used to achieve the required suppression.

For the first loop, a small sample of light is picked off from the pre-modecleaner cavity; audio-band intensity fluctuations in this beam are sensed with a pair of photodiodes, producing an electronic error signal. This error signal is fed back to a single-pass AOM placed directly in the path of the main high-power beam. The loop has a bandwidth of approximately 50 kHz and stabilizes the RIN of the beam to a few parts in $10^{-8}/\mathrm{Hz}^{1/2}$ between 30 Hz and 1 kHz [11].

To provide further intensity noise suppression, a second loop is employed using a sample of the light transmitted through the input modecleaner. This loop has a bandwidth of approximately 10 kHz and is designed to produce a RIN of $2\times10^{-9}/\mathrm{Hz}^{1/2}$ at 10 Hz. Similar to the frequency noise, the intensity noise is passively filtered by the common-mode cavity above 0.6 Hz.

V. INTERFEROMETER SENSING AND CONTROL

Sensing of the interferometer's length and angle degrees of freedom is accomplished via a combination of rf (PDH-type) readout and dc signals. To facilitate rf readout, 9.1 MHz and 45.5 MHz phase sidebands are applied with an electro-optic modulator (EOM) placed before the interferometer input. The macroscopic lengths between the interferometer optics have been chosen so that the 9.1 MHz sidebands resonate between the power-recycling mirror and the input test masses, and the 45.5 MHz sidebands resonate between the signal-recycling mirror and the input test masses.

A. Lengths and angles

The interferometer's common-mode arm length is left uncontrolled in the GW band, since it serves as a length reference for the laser. Below a few hertz, common-mode length control is applied to the end test mass suspensions in order to offload low-frequency control signal accumulated on the reference cavity AOM. This low-frequency control amounts to a few hundred microns of motion per day, and arises from earth tides, static radiation pressure on the test masses, and thermally induced drifts in the tabletop reference cavity length.

Differential arm length motion is sensed with a variant of homodyne readout [16]: a small differential length offset ($\simeq 13$ pm at 25 W of input power) is applied to one of the test masses, which causes carrier light to leak out the antisymmetric port, pass through the output modecleaner, and impinge on the GW photodetectors. Differential test mass motion produces audio-frequency sidebands which beat against the dc offset light, creating intensity fluctuations on the GW photodetectors. This signal is used both as an estimate of the GW strain $h(t)$, and as an error signal for controlling the differential arm length. It is fed back to one of the end test masses, forming a control loop with a bandwidth of approximately 45 Hz.

The positions of the power- and signal-recycling mirrors and of the beamsplitter are sensed via PDH using a photodiode that monitors the light circulating in the power recycling cavity. These loop bandwidths range from 10 to 60 Hz.

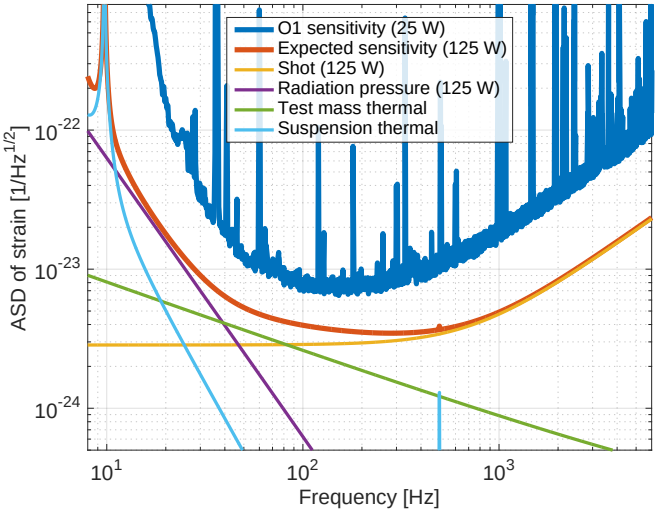

FIG. 2: Advanced LIGO differential strain sensitivity curves, showing the actual performance of the Hanford detector during the first observing run (the Livingston performance is similar), the expected performance of the detectors at full design sensitivity, and contributions to the full design sensitivity from shot noise, radiation pressure noise, and thermal noises.

The interferometer has 20 angular degrees of freedom which are sensed interferometrically [17]. The angular motion of the test masses presents a particularly challenging control problem. The light stored in the interferometer arms generates optical torques which couple the test masses, producing modes which either soften or harden the torsional modes of the test mass suspensions in a power-dependent way [18].

B. Mode shape

The interferometer's mirrors are intentionally curved, thereby keeping the spatial mode of the resonating beam well-defined. A thermal compensation system is employed in order to adjust this mode [19]. The curvature of each test mass can be fine-tuned by resistively heating a coil of nichrome wire mounted close to the test mass barrel; the thermal radiation from this wire is absorbed in the test mass substrate. This also provides a mechanism for avoiding parametric instabilities which arise from the interaction of test mass body modes with higher-order optical modes [20]. Additionally, antireflection-coated fused silica compensation plates placed between the beamsplitter and each input test mass may be heated using a CO_2 laser; a mask placed between the laser and the plate determines the geometry of the applied heating.

VI. NOISE PERFORMANCE DURING FIRST OBSERVING RUN

During the first observing run, the high-power injection-locked amplifiers were not used, and the interferometers were illuminated with about 25 W of laser light, yielding 100 kW of circulating power in each arm [21]. Additionally, a 37 % transmissive signal recycling mirror was used. The differential strain ASD was less than $10^{-23}/\mathrm{Hz}^{1/2}$ between 100 and 300 Hz (fig. 2). The strain ASD was limited by shot noise above 200 Hz, control noise from other degrees of freedom below 30 Hz [22]. The limiting noise source between 30 Hz and 200 Hz is not yet known.

VII. FUTURE PLANS

Interferometer commissioning is ongoing, with a current focus on operating with more than 25 W of input power. This requires changes to the angular control system, reconfiguration of the thermal compensation system, and new electrostatic damping infrastructure to combat the increased number of parametric instabilities. A second astrophysical observing run is planned to start before the end of 2016.

Longer-term improvements to Advanced LIGO may include frequency-dependent squeezed light to reduce the quantum noise, heavier test masses to reduce radiation pressure noise, better coating materials to reduce the test mass thermal noise, or longer suspensions to reduce suspension thermal noise [23].

ACKNOWLEDGMENTS

LIGO was constructed by the California Institute of Technology and Massachusetts Institute of Technology with funding from the National Science Foundation and operates under cooperative agreement PHY–0757058. This paper has the internal project designation LIGO–P1600132.

[1] J. D. E. Creighton *et al.*, *Gravitational-Wave Physics and Astronomy* (Wiley-VCH, 2011).
[2] B. P. Abbott *et al.*, Phys. Rev. Lett. **116**, 061102 (2016).
[3] B. P. Abbott *et al.*, Phys. Rev. Lett. **116**, 241103 (2016).
[4] J. Aasi *et al.*, Class. Quantum Grav. **32**, 074001 (2015).
[5] A. Buonanno *et al.*, Phys. Rev. D **64**, 042006 (2001).
[6] J. Mizuno, Ph.D. thesis, Universität Hannover (1995).
[7] D. V. Martynov, Ph.D. thesis, California Institute of Technology (2015).
[8] M. Evans *et al.*, Phys. Rev. D **78**, 102003 (2008).
[9] G. M. Harry *et al.*, Class. Quantum Grav. **24**, 405 (2007).
[10] A. V. Cumming *et al.*, Class. Quantum Grav. **29**, 035003 (2012).
[11] P. Kwee *et al.*, Opt. Express **20**, 10617 (2012).
[12] L. Winkelmann *et al.*, Applied Physics B **102**, 529 (2011).
[13] R. W. P. Drever *et al.*, Applied Physics B **31**, 97 (1983).
[14] R. Adhikari *et al.*, Tech. Rep. LIGO-T070236 (LIGO, 2008).
[15] T. Chalermsongsak *et al.*, Metrologia **52**, 17 (2015).
[16] T. T. Fricke *et al.*, Class. Quantum Grav. **29**, 065005 (2012).
[17] L. Barsotti *et al.*, Class. Quantum Grav. **27**, 084026 (2010).
[18] J. A. Sidles *et al.*, Physics Letters A **354**, 167 (2006).
[19] A. Brooks *et al.*, In prep. (2016).
[20] M. Evans *et al.*, Phys. Rev. Lett. **114**, 161102 (2015).
[21] B. P. Abbott *et al.*, Phys. Rev. Lett. **116**, 131103 (2016).
[22] D. V. Martynov *et al.*, Phys. Rev. D **93**, 112004 (2016).
[23] J. Miller *et al.*, Phys. Rev. D **91**, 062005 (2015).